Available online at www.sciencedirect.com
SCIENCE DIRECT
Flow Measurement and Instrumentation 17 (2006) 59–68
Flow Measurement and Instrumentation
www.elsevier.com/locate/flowmeasinst

Synchronous measurements of the velocity and concentration in low density turbidity currents using an Acoustic Doppler Velocimeter

S.A. Hosseini, A. Shamsai, B. Ataie-Ashtiani*

Department of Civil Engineering, Sharif University of Technology, P.O. Box: 11365-9313, Tehran, Iran

Received 23 December 2004; received in revised form 28 April 2005; accepted 13 May 2005

Abstract

Low density turbidity currents have been investigated in a laboratory flume. An Acoustic Doppler Velocimeter (ADV) was used to measure the velocity. The dimensionless velocity profiles were compared with previous studies to check the accuracy of acoustic measuring techniques for turbidity currents. Successful use of the ADV to measure the current velocity has led to interest in the technique of using acoustic sensors to estimate concentrations. Acoustic backscattering analyses are used for estimating the sediment concentration in turbidity currents. With this approach, concentration measurements can be reasonably well represented by a similarity profile. Using this technique, an accurate estimation of the concentration close to the bed, where obtaining reliable concentration data by sampling techniques is difficult, is possible. The results show that a power relation is a good estimate for the concentration distribution in this region, for which no reliable expressions have been provided previously.

Successful estimation of the velocity and concentration, in the present experiments, indicates that this technique could be appropriate and useful for determining the flow structure in turbidity currents.

Keywords: Turbidity current; Acoustic Doppler Velocimeter; Velocity measurement; Sediment concentration; Backscattering analyses

1. Introduction

Gravity or density currents are flows driven by density differences. Turbidity currents are types of gravity currents where the driving force is gained from suspended sediments and turbid water made heavier than the clear water above it. Geological observations show turbidity currents to be a common form of sediment transport in many sedimentary basins (lakes, reservoirs, seas, oceans, etc.) [1].

Unfortunately, natural turbidity currents are hard to observe and study, owning to their large-scale and often destructive nature [1]. So, experimental study is one of the best means of understanding the dynamics of gravity currents. A large number of experimental studies on gravity currents can be seen in the literature [2–12].

Various methods have been considered for measuring flow velocity in sediment-laden gravity currents. Flow measurements were carried out primarily using intrusive equipment that disturbed the flow, e.g. micropropeller current meters [2,11,12], and so only mean flow properties were determined rather than turbulent velocity measurements. Using a hot film probe fails due to particle impingement on the sensor so this instrument is usually used in saline density currents [13]. Instantaneous velocity measurements have been made using dyed material [13], Laser-Induced Fluorescence (LIF) [14], and electromagnetic current meters [15] but one of the limitations is due to their spatial resolution [16].

In recent years the application of new experimental techniques, such as Laser Doppler Anemometry (LDA), use of the Acoustic Doppler Velocimeter (ADV), and Ultrasonic Doppler Velocity Profiling (UDVP), has allowed turbulent velocity measurements. LDA does not operate in turbid water because incident laser beams are rapidly attenuated

* Corresponding author. Tel.: +98 21 6164186; fax: +98 21 6014828.
E-mail address: ataie@sharif.edu (B. Ataie-Ashtiani).

0955-5986/$ - see front matter © 2005 Elsevier Ltd. All rights reserved.
doi:10.1016/j.flowmeasinst.2005.05.002

and the light diffused by the particles is spread when the sediment concentration is a few hundred milligrams per liter. LDA operates in saline density currents efficiently [5–7]. The ADV is attractive for measuring instantaneous velocities, while it is non-intrusive remote sensing system. In recent years it has been replacing previously developed flow meters (e.g. electromagnetic current meters, propeller meters, hot film and hot wire) after validation through comparison with them [14,17].

Measurements of concentration in gravity currents have also been carried out and the general characteristics of the concentration profiles have been described [4,12]. Conventional methods for measuring concentration require routine sample collection at different heights in the current and subsequent analysis of the water samples [2,10–12]. However these methods are not safe and are increasingly being forsaken in favor of accurate and safe methods for real time monitoring of sediment concentration.

Acoustic backscattering measurement is non-intrusive technique for determining sediment concentration with a high degree of temporal and spatial resolution [18–21]. Acoustic backscattering measurements of suspended sediments have been used in marine, ocean, open channel flow, and fluvial environments [22–25].

The objectives of this paper are to study experimentally the physical structure of continuous and weakly depositional turbidity currents with an emphasis on the velocity and concentration structure, using the ADV technique. Moreover, the appropriateness and accuracy of the ADV technique for this kind of flow are investigated. Applying backscattering analysis, measurement of the concentration without interfering with the current and synchronized to velocity data gathering is tried.

2. Experimental set-up and procedure

A laboratory apparatus was designed to study the structure of three-dimensional, inclined turbidity currents. The experimental set-up is illustrated in Fig. 1. Turbid water is continuously released from an opening with a rectangular cross section and spreads down a sloping surface in a tank of fresh water. A Plexiglas gate controls the opening. The size of the opening can be regulated with a gate. In all the experimental runs, the opening was set to 1 cm high and 10 cm wide. The entire tank is divided into two sections. The shorter upstream section is an inlet box with an opening in the middle of it for introducing the denser fluid to produce a current.

The turbid water is released from a gate valve on the supply pipe into the inlet box. The input rate is controlled by a flow meter and fixed at a constant rate. In this way, the current could be in a quasi-steady condition. The second section of flume is the reservoir or basin in which the density current is found and the measuring sections are located. The slope of this section (basin) can be adjusted in the range of 0% to 3%.

A mixing tank with a maximum capacity of 2 m^3 was used to prepare a mixture of sediment and water. When the sediment was thoroughly mixed with water in the mixing tank, a gate valve on the supply pipe was opened and the experiment was started by allowing the dense fluid (suspension) to flow into the main tank and the turbidity current generated. At the end of the tank the turbid water was drained out thorough the bottom drain.

In all of the experiments, kaolin with the specific gravity of 2.65 was used as the suspended material. The mean particle diameter is $D_{50} = 0.02$ mm. The mean falling velocity of the suspended sediments, calculated through the empirical relation proposed by Dietrich [26], is $V_s = 0.36$ mm/s. The initial bulk density of the dense fluid is less than 1008 kg/m^3, in all experiments, and the mixture is considered as a Newtonian fluid.

The total of 27 successful experiments are carried out. The initial conditions for the experiments, as well as some of the experimental results, are summarized in Table 1. Inlet conditions include: slopes; sediment concentration C_0; flow discharge Q; flow velocity U_0; and reduced gravity g'_0.

Fig. 2 shows the pattern of longitudinal and lateral spreading of the turbidity current after its initial release. Longitudinal (x), transverse (y), and vertical (z) directions are shown in Fig. 2. The advancing front disturbs and entrains the surrounding fluid during spreading and a uniform, steady (quasi-steady) flow take place upstream of the front (in the body of the current), as shown in Fig. 2. It is also observed that the body height of the current remains relatively constant along the basin length. The height of the body is approximately constant. Flow velocities are measured in the steady dense layer flow (body) behind the initial front (head). Velocities are measured simultaneously in two vertical profiles at 5.0 and 6.0 m from the opening where entrance disturbances and reflections at the outlet have no influence on the measurements. Two ADV's are mounted on the carrier, used for measurement. Measurements in the body of the current with ADV's began when the head of the current reached the end wall of the basin. After 20–30 s of data acquisition, the probes are moved downward to the next measurement position until the profile is completed. The total duration of each experiment is about 60 min. The ADV measurements are supplemented with direct water sampling with siphoning in order to obtain the suspended sediment concentration.

These series of experiments were carried out to obtain instantaneous velocities, mean flow properties, and velocity profiles without interfering in the turbidity currents. Also, using backscattering analysis and signal amplitude comparison, concentration profiles were obtained for these experiments.

3. Acoustic Doppler Velocimeter and measurements

The ADV is attractive for measuring instantaneous velocities, while it is a non-intrusive remote sensing

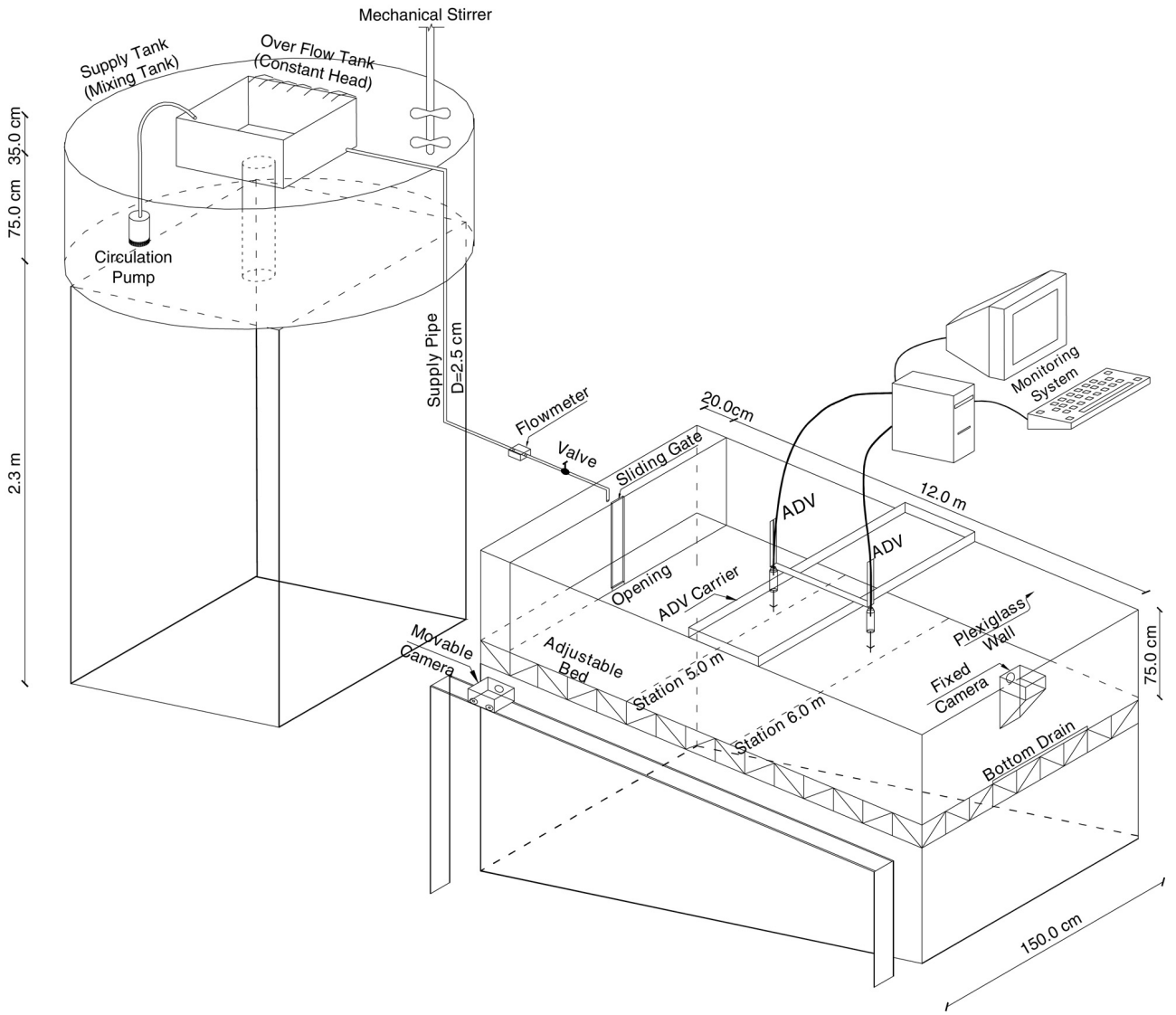

Fig. 1. Three-dimensional view of the experimental set-up.

system. ADV's can fulfill the roles of other flow meters, including electromagnetic current meters, propeller meters, hot film and hot wire probes [14,17]. It is a useful tool for measuring all three components of velocity in laboratory and field environments [24,27]. This instrument is commercially available and in recent years it has been replacing the previously developed flow meters. ADV's have quickly become valuable tools for laboratory and field investigations of river flow, canals, reservoirs, oceans, and around hydraulic structures and laboratory scale models. This instrument is relatively rugged, easy to operate and can be readily mounted and maneuvered with the flow field.

A 10 MHz 5 cm Nortek acoustic Doppler velocimeter was used for measuring velocities in the experimental runs. It uses a technique known as pulse-to-pulse coherent Doppler sonar for measuring the velocity vector [28]. The phase shift between successive backscattered signals sampled at each receiver is converted to a measurement of velocity along each beam. Factory calibration of the ADV permits conversion of along-beam velocity into an orthogonal coordinate system. The error in the prediction of mean velocities is no greater than ± 2.5 mm/s $\pm 1\%$. Other performance characteristics are as follows: acoustic frequency 10 MHz; velocity range ± 0.03, 0.10, 0.30, 1.0, or 2.5 m/s; velocity resolution 0.1 mm/s; velocity bias $\pm 0.5\%$ with no measurable zero-offset in the horizontal direction; sampling rate between 0.1 and 25 Hz; random noise approximately 1% of the velocity range at 25 Hz sampling rate; sampling volume less than 0.25 cm^3; minimum distance from the sampling volume to the boundary 5 mm [28].

An important advantage of the ADV is its ability to measure the flow in a small sampling volume (approximately 0.25 cm^3) that is located 5 (or 10) cm away from the sensing elements. So, although the probe is inserted into the flow, the sensing volume is several centimeters away from all

Table 1
Summary of the initial conditions and the experimental results

Exp. no.	Slope (%)	C_0 (g/cm^3)	Q (l/min)	U_0 (cm/s)	g_0' (cm/s^2)	H_m (cm)	U_m (cm/s)	H_t (cm)	U (cm/s)	H (cm)	Re	Ri	Fr'
No. 1	3	0.005	15.0	25.00	1.89	4.2	1.9	12.60	1.43	9.70	1275.9	8.99	0.33
No. 2	3	0.005	8.0	13.33	1.89	3.35	1.45	10.30	1.12	8.00	824.2	12.08	0.29
No. 3	3	0.005	4.0	6.67	1.89	1.66	0.6	5.60	0.46	4.30	181.9	38.49	0.16
No. 4	3	0.01	16.5	27.50	3.30	3.3	2.58	11.10	1.99	8.60	1546.5	7.16	0.37
No. 5	3	0.01	12.0	20.00	3.82	2.55	2.42	9.30	1.83	7.15	1229.9	8.16	0.35
No. 6	3	0.01	3.0	5.33	3.82	1.43	0.68	4.90	0.51	3.80	182.2	55.81	0.13
No. 7	3	0.01	4.5	7.50	3.64	1.7	1.25	6.00	0.95	4.70	414.2	18.97	0.23
No. 8	3	0.015	20.0	33.33	4.11	3.6	3.361	11.80	2.55	9.10	1910.9	5.75	0.42
No. 9	3	0.015	15.0	25.00	4.70	2.8	2.9	9.50	2.20	7.25	1416.3	7.04	0.38
No. 10	3	0.015	10.0	16.67	4.44	1.85	2.35	6.40	1.80	4.90	762.4	6.72	0.39
No. 11	2	0.005	10.0	16.67	1.43	3.4	1.487	10.60	1.12	8.20	812.3	9.36	0.33
No. 12	2	0.005	15.0	25.00	1.56	4.8	1.85	14.50	1.42	11.30	1438.5	8.74	0.34
No. 13	2	0.005	20.0	33.33	1.73	5.8	1.93	20.00	1.49	15.30	2071.6	11.88	0.29
No. 14	2	0.01	10.0	16.67	3.64	2.45	1.68	8.30	1.26	6.32	738.6	14.50	0.26
No. 15	2	0.01	15.0	25.00	3.00	3.3	2.6	11.30	1.98	8.75	1525.0	6.70	0.39
No. 16	2	0.015	10.0	16.67	4.87	2.13	2.15	6.90	1.63	5.37	787.2	9.84	0.32
No. 17	2	0.015	15.0	25.00	4.87	3.65	2.837	11.10	2.12	8.55	1630.1	9.26	0.33
No. 18	2	0.015	20.0	33.33	4.87	4.2	3.187	13.00	2.40	10.05	2169.2	8.49	0.34
No. 19	1	0.005	10.0	16.67	1.56	3.85	1.325	12.00	1.02	9.27	847.4	13.90	0.27
No. 20	1	0.005	15.0	25.00	1.56	6.1	1.67	18.20	1.29	14.20	1642.1	13.31	0.27
No. 21	1	0.005	20.0	33.33	1.24	6.7	1.75	22.20	1.33	17.10	1948.9	12.00	0.29
No. 22	1	0.01	10.0	16.67	3.08	3.12	1.69	10.80	1.27	8.27	932.0	15.78	0.25
No. 23	1	0.01	15.0	25.00	2.78	3.5	2.15	12.20	1.66	9.40	1321.1	9.49	0.32
No. 24	1	0.01	20.0	33.33	3.13	6.25	2.25	20.70	1.73	16.40	2531.3	17.15	0.24
No. 25	1	0.015	10.0	16.67	5.39	2.4	1.8	8.40	1.35	6.43	812.0	19.02	0.23
No. 26	1	0.015	15.0	25.00	4.70	3.3	2.6	11.30	1.96	8.60	1496.6	10.52	0.31
No. 27	1	0.015	20.0	33.33	4.87	3.57	3.25	12.35	2.44	9.30	2040.7	7.60	0.36

physical parts of the probe; therefore the presence of the probe generally does not disturb the measurement. This is an important advantage for studying density currents, because the sensing element is placed in calm water (ambient fluid) and measures the velocity of the current beneath itself.

There are three limitations when applying ADV's in sediment-laden flow (turbidity currents) that require additional considerations. Firstly, the ADV (like any acoustic sensor) measures the velocity of acoustic targets (e.g. solid particles) but not the fluid velocity. It is assumed that the sediment and fluid travel at the same velocity. This assumption is likely to be valid only when considering fine sediment, dominantly in suspension, as in our study. For coarser particles (e.g. sand) this effect may introduce additional uncertainty [17,22,24]. The second problem is the spatial changes in density and density stratification within the current and therefore change in the acoustic velocity. Whereas the sediment concentration in dense fluid has a value up to 3% (or 15 g/l) and the density of the dense fluid at this concentration is approximately 1008 kg/m^3, the change in acoustic velocity is not an inherent problem and is less that the error limits within this technique [17] for these cases. Thirdly, when the sediment concentration increases up to 50 g/l, acoustic waves are absorbed in sediment-laden flow and attenuated. So the ADV cannot operate properly.

The right-handed coordinate system was used in measurements and data analysis. The coordinate system is as follows: x positive downstream along the main flow (velocity component u), y positive in the cross stream direction oriented to the left bank (velocity component v), and z positive upward toward the water surface (velocity component w).

The instantaneous velocity recorded by ADV probes should be checked for unreliable data and if necessary corrected before calculating the flow characteristic. Finally, corrected velocity data were used to calculate the mean flow properties. Mean velocities are calculated from the temporal averaging of the recorded time series at each point.

4. Experimental results and analysis

4.1. Mean velocity profile

Many researchers have described the general characteristics of the velocity profiles of density currents previously [4,7,10]. A typical profile of a downstream velocity and some terms used to define density currents are shown in Fig. 3 [7]. Experimental studies have shown that the velocity profile in gravity currents has a shape similar to that of wall jets. So the gravity currents include two regions: an inner region and an outer region that are separated through the maximum velocity (U_m). The inner region (wall region) has a positive velocity gradient and the outer region has a negative velocity gradient that reflects the backflow of ambient fluid.

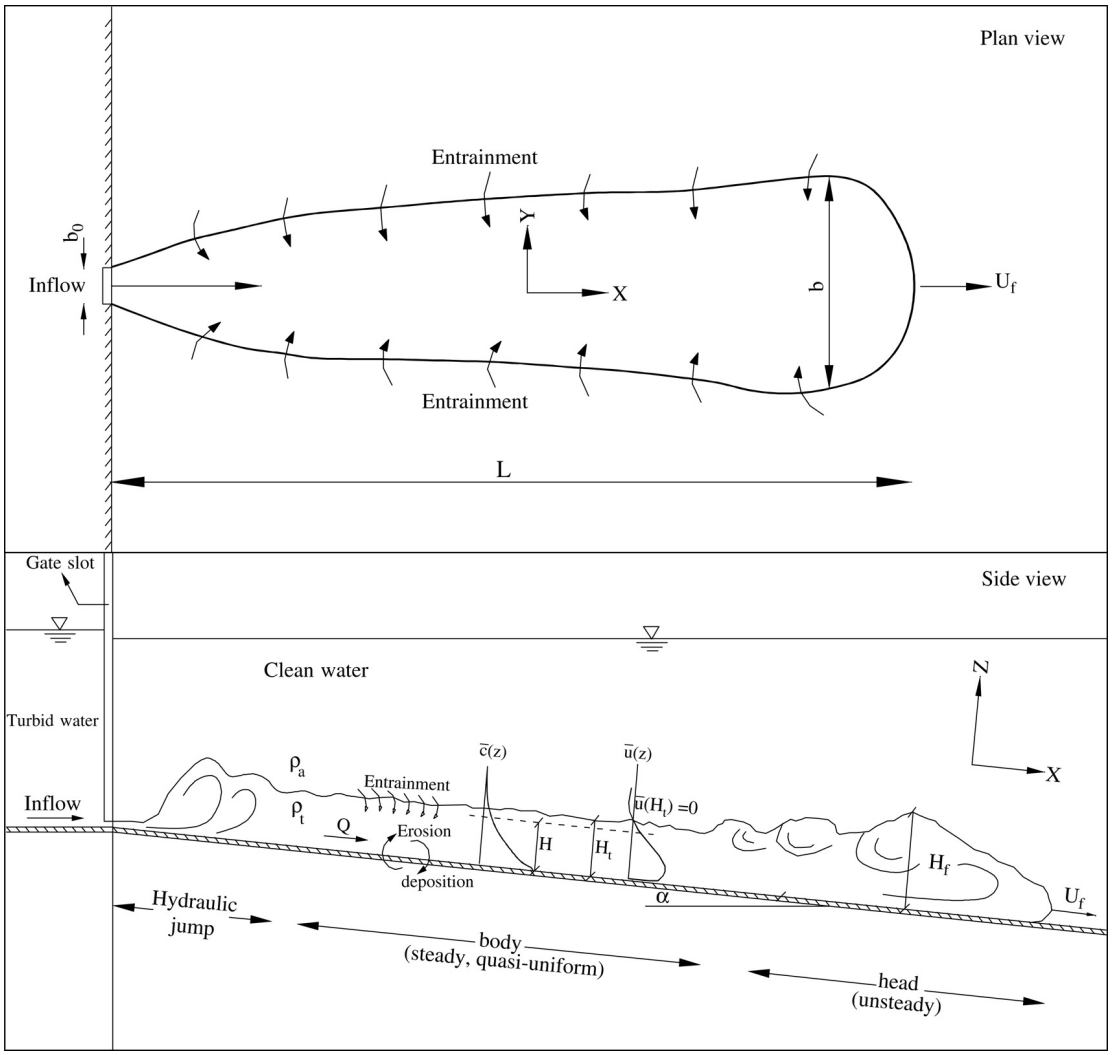

Fig. 2. The pattern of longitudinal and lateral spreading of a three-dimensional turbidity current advancing on a slope.

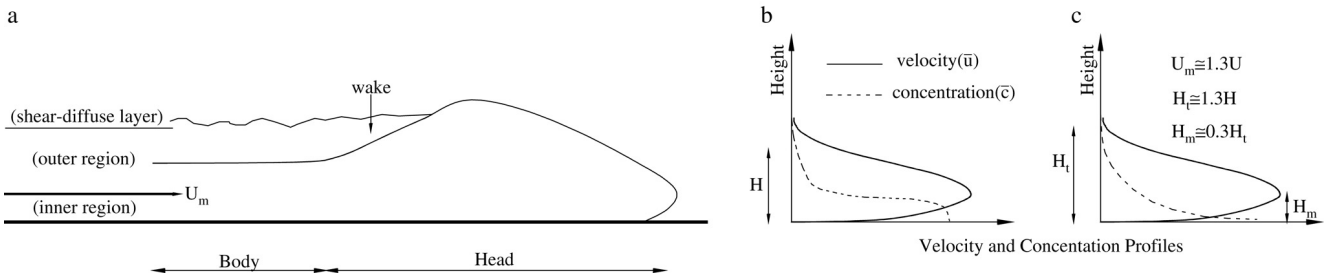

Fig. 3. Sketch of defined regions in density currents and a typical profile of downstream velocity and mean concentration.

The mean downstream velocity ($\overline{u}$) was calculated by temporal averaging of the recorded time series at each point for all of the vertical profiles. The velocity maximum (U_m), as the characteristic velocity, and the height of the velocity maximum (H_m) and the depth-averaged thickness of the current (H), as length scales, were used to obtain the non-dimensional form of the velocity profiles [10]. Dimensionless velocity profiles are shown in Fig. 4a. As seen, velocity distributions can be reasonably well represented by similarity profiles. The upper and lower boundary drag and shear at these two boundaries and the velocity gradient affect the velocity profile; so the total profile was separated into two parts and the flow behavior in each region was considered for the proposed profiles.

Within the inner region of current that is placed below the velocity maximum (U_m), the drag at the lower boundary

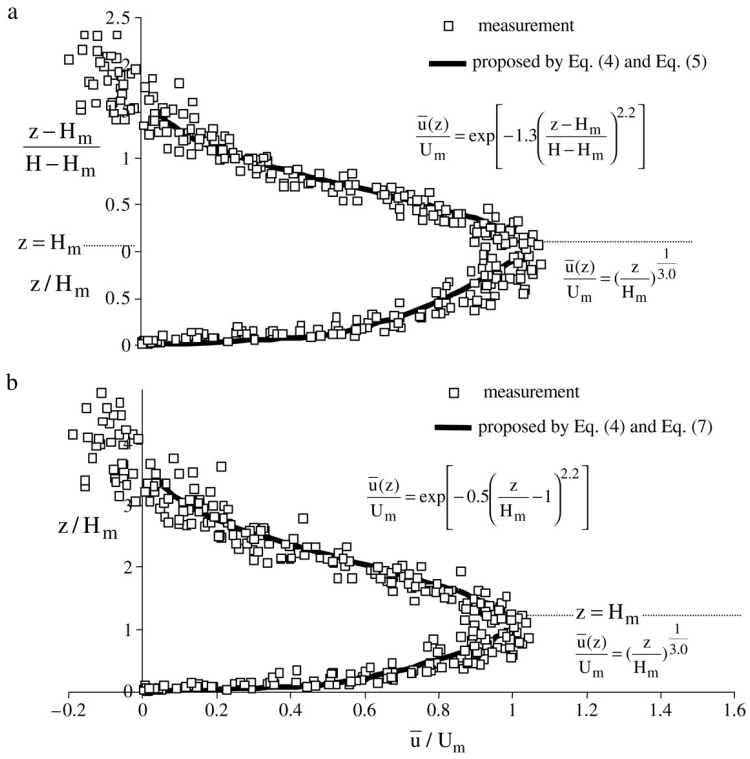

Fig. 4. Dimensionless velocity profile.

is the main parameter and the expression for the velocity profile is a logarithmic relation, as follows [7,10]:

$$\frac{\overline{u}(z)}{u_*} = \frac{1}{k}\ln z + \text{ Cons.} \tag{1}$$

The logarithmic velocity profile can be simplified to an empirical power relation [10]:

$$\frac{\overline{u}(z)}{U_\mathrm{m}} = \left(\frac{z}{H_\mathrm{m}}\right)^{\alpha_v} \tag{2}$$

where U_m is velocity maximum, H_m is height of velocity maximum, $\overline{u}(z)$ is mean downstream velocity at distance z above the bed, and α_v is empirical exponent.

The effect of the upper drag boundary on the velocity profile was modeled by a density-stratified layer of finite thickness between two homogeneous fluids [7]. The velocity distribution in the outer region is given by a near-Gaussian relation [10]:

$$\frac{\overline{u}(z)}{U_\mathrm{m}} = \exp\left[-\beta_v\left(\frac{z-H_\mathrm{m}}{H-H_\mathrm{m}}\right)^{\gamma_v}\right] \tag{3}$$

where β_v is a coefficient, γ_v is an empirical exponent and H is the depth-average thickness of current.

Eqs. (2) and (3) were fitted to the velocity profiles measured inside the inner and outer regions for different experimental cases. Best-fit curves with respect to the exponents (α_v and γ_v) and coefficient (β_v) were obtained using the least squares method. The results of these curve fits show that α_v, γ_v, and β_v have values in the ranges of 0.24 to 0.42, 1.9 to 2.6, and 1.2 to 1.6, respectively. If average values of these coefficients are used, the inner and outer vertical profiles are simplified as follows:

$$\frac{\overline{u}(z)}{U_\mathrm{m}} = \left(\frac{z}{H_\mathrm{m}}\right)^{0.34} \tag{4}$$

$$\frac{\overline{u}(z)}{U_\mathrm{m}} = \exp\left[-1.3\left(\frac{z-H_\mathrm{m}}{H-H_\mathrm{m}}\right)^{2.2}\right]. \tag{5}$$

Comparison between the depth-average height of the current (H) and the height of the velocity maximum (H_m) in the next section shows that

$$H = 2.6H_\mathrm{m} \tag{6}$$

and Eq. (5) is simplified to

$$\frac{\overline{u}(z)}{U_\mathrm{m}} = \exp\left[-0.5\left(\frac{z}{H_\mathrm{m}}-1\right)^{2.2}\right]. \tag{7}$$

Summation of Eqs. (7) and (4) (or (2) and (3)) can yield a profile for the entire flow:

$$\begin{cases} \nu(\eta) = (\eta)^{0.34}\psi(1-\eta) \\ \qquad\quad + \exp\left[-0.5\,(\eta-1)^{2.2}\right]\psi(\eta-1) \\ \psi(1-\eta) = \begin{cases} 1 & \eta < 1 \\ 0 & \eta > 1 \end{cases} \end{cases} \tag{8}$$

where $\eta = \frac{z}{H_\mathrm{m}}$, $\nu = \frac{\overline{u}}{U_\mathrm{m}}$ and ψ is the unit step function or Heaviside function.

Measured dimensionless velocity profiles have been compared with the proposed velocity profile of Eq. (8) in

Fig. 4b. Good agreement between the values of Eq. (8) and measured data can be observed.

On the basis of the measurements, three regions are defined for the gravity current (Fig. 3a): the inner region between the bed and velocity maximum, the outer region between the velocity maximum and zero velocity, and a shear–diffusion layer where the particles are affected by shear and diffusion. In this paper a new region in velocity profiles is introduced. Velocity values in this region have negative values ($\overline{u} < 0$). The proposed velocity profile given by the above equation (Eq. (8)) is valid only up to the outer region where the velocity is approximately equal to five per cent of the velocity maximum. The dimensionless velocity profile shows that measurement data inside the shear–diffusion layer exhibit large scattering; thus no equation can be suggested for this region.

4.2. Depth-averaged flow parameters

The depth-averaged velocity (U) and the thickness of the turbidity currents (H) can be calculated from the measured velocity profiles using the following equations [9]:

$$UH = \int_0^\infty \overline{u}(z)\mathrm{d}z = \int_0^{H_t} \overline{u}(z)\mathrm{d}z \tag{9}$$

$$U^2H = \int_0^\infty \overline{u}^2(z)\mathrm{d}z = \int_0^{H_t} \overline{u}^2(z)\mathrm{d}z \tag{10}$$

where $\overline{u}(z)$ is the mean downstream velocity at distance z above the bed, and H_t is the height at which $\overline{u}(H_t) \approx 0$.

The calculated averaged velocity (U) and height (H) for different experiments are summarized in Table 1. The derived values were used to calculated the flow Reynolds number (Re) and the bulk Richardson number (Ri):

$$Re = \frac{\rho_0 U H}{\mu} \tag{11}$$

$$Ri = \frac{g_0' H}{U^2} \tag{12}$$

$$g_0' = \frac{g(\rho_0 - \rho_a)}{\rho_a} \tag{13}$$

where ρ_0 is the initial current density, μ is the dynamic viscosity and g_0' is the initial reduced gravitational acceleration, and ρ_a is the ambient density.

From the measured velocity profiles, the velocity maximum (U_m), total current thickness (H_t), and the height of the velocity maximum (H_m) were extracted and these are summarized in Table 1. The ratios between $\frac{U_m}{U}$, $\frac{H_t}{H}$, and $\frac{H_m}{H_t}$ were also calculated. The average values of these parameters are as follows:

$$\frac{U_m}{U} \approx 1.3 \tag{14}$$

$$\frac{H_t}{H} \approx 1.3 \tag{15}$$

$$\frac{H_m}{H_t} \approx 0.3. \tag{16}$$

These results are in good agreement with the values obtained by previous studies [10,17].

4.3. Estimation of mean concentration

One of the most widely measured parameters of density currents is the concentration. Concentration measurements for suspended sediments are crucial to the study of erosion and deposition processes.

The ADV works by measuring the reflection of an acoustic signal from particulate matter in water. While this instrument is primarily used to measure the velocity of the particles, it can also provide information about the quantity of sediment present. This information is measured in the form of the intensity of the reflections received, also referred to as the backscattering strength or signal amplitude [29].

A standard ADV system provides a signal amplitude, as part of its output record, which is measured with the same frequency and in the same sampling volume as the velocities. The Signal Amplitude (SA) value obtained by the ADV is proportional to the logarithm of the intensity of the acoustic signal that is backscattered from small particles within the sampling volume. The intensity backscattered by particles in the sampling volume, I, is estimated using [22–25,27]

$$I \propto 10^{0.0434\mathrm{SA}}. \tag{17}$$

In this study, I is given as the average of three intensity values obtained by three receivers. The backscattered intensity, I, is a function of the particle type, concentration and size of particles. The simplified relation between the intensity, I, and sediment concentration, c, can be expressed as

$$I = \frac{I_0 c S_f S_a \exp[-2r(\alpha_w + \alpha_s)]}{r^2} \tag{18}$$

where I_0 is the transmitted intensity, c is the mass sediment concentration, S_f contains all system specific parameters such as transducer size, efficiency, probe geometry, and receive sensitivity, S_a holds all the particle specific parameters (size, elasticity, and density), α_w is the water absorption, α_s is the absorption due to particle scattering, and r is the acoustic propagation path.

For low concentration, the particle attenuation is negligible. Since the acoustic frequency of the ADV is high (10 MHz), α_w is constant, approximately. So, there is a nearly linear relationship between the concentration (c) and intensity (I). Outside the linear range, the intensity is a non-linear function of the concentration and the values should not be used for sediment analysis. General experience indicates that the linear region corresponds to a sediment concentration of about 10 g/l [29].

For the experiments of the present work, initial concentrations have values up to 15 g/l, but through lateral and vertical entrainment, the concentration reduces and in the working section it would be below the limit. Collected samples prove that the concentration values are less than 10 g/l after the spreading of turbid water.

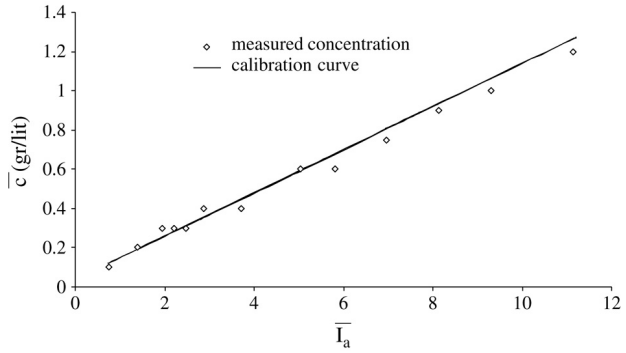

Fig. 5. Relationship between acoustic backscattering intensity and mass sediment concentration.

So, based on the above illustrations, the intensity of the acoustic signal (I) from sediment particles within the ADV sampling volume can be used as a surrogate measurement of suspended sediment concentration in experiments. We simplify Eq. (18) for low concentration results:

$$I_a \propto c \propto (10^{0.0434SA_1} + 10^{0.0434SA_2} + 10^{0.0434SA_3}) \qquad (19)$$

where SA_1, SA_2, and SA_3 are the signal amplitudes obtained by three receiving transducers and I_a is the average of three intensity values obtained by three receivers.

The acoustic backscattering intensity of the ADV was calibrated in the laboratory, using the sediment concentration measured conventionally from the siphon sampling. The concentration was measured by siphon sampling at the middle height of the currents. The collected samples were oven dried and weighted for determining the concentration. The measured concentration was used for producing a calibration curve relating backscattering intensity and sediment concentration.

Fig. 5 shows the relationship between the mean of the averaged acoustic intensity ($\overline{I}_a$) and the mean of the mass sediment concentration ($\overline{c}$). As seen, the calibration curve is almost linear with zero offset. So we have

$$\overline{c} = \lambda \overline{I}_a \qquad (20)$$

where λ is the calibration coefficient and is unique to each ADV.

The coefficient λ is primarily influenced by particles in the size range of 0.02–0.1 mm, as the ADV is most sensitive to this range, and these can be considered as ideal backscattering media [24,25]. This range of particles (0.02–0.1 mm) overlaps the dominant range of suspended particles used in this study. The same technique has been successfully used by Thevenot et al. [30], Kawanisi et al. [22, 23], and Nikora et al. [24,25] to study sediment dynamics.

In this paper Eq. (20) was used to determine the mean sediment concentration at different heights above the bed. In all cases the flow is density stratified. A dense basal layer with high density gradient can be observed in the lower part of the flow (from the bed to the depth-averaged current thickness $0 < z < H$), and a more homogeneous, well-mixed fluid with a lower density exists at the top (upper average current thickness $z > H$).

The general characteristics of the concentration profiles have been described previously [2,4,10]. All these measurements are based on a point sampler using siphoning. As shown in Fig. 3, the concentration measurements of both turbidity currents [2,10,11] and saline currents [5,9] present two main types of sediment concentration distributions. The first type of concentration distribution has a stepped concentration profile (Fig. 3b) and usually occurs in erosional currents [11] or for currents inferred with high entrainment rate at the upper boundary [4]. The second type of concentration profiles are smooth profiles (Fig. 3c), and are commonly seen in low concentration, weakly depositional current or in saline currents [2,9,10]. The maximum density gradient in these currents is observed near the base of the current, decreases around the averaged current height (H), and reaches zero at the total current thickness (H_t) and in shear–diffusion layer.

The height of the velocity maximum (H_m) and the concentration at this height (C_m) are used to obtain dimensionless forms of concentration profiles. Dimensionless concentration profiles for the experiments conducted are shown in Fig. 6a. As seen, the concentration distribution can be represented by similarity profiles as well as the velocity. The overall shape of the concentration profiles is in good agreement with published results for saline or weakly depositional turbidity currents (Fig. 3c) [4,10]. Nearly no sediment depositions were observed at the end of the experimental runs.

Similar to the velocity profile case, two expressions are suggested for concentration profiles in the inner and outer regions. Within the inner region of current that is placed below velocity maximum, (U_m), the expression for the concentration is an empirical power relation as the velocity profile:

$$\frac{\overline{c}(z)}{C_m} = \left(\frac{z}{H_m}\right)^{-\alpha_c} \qquad (21)$$

where α_c an empirical exponent; C_m is the mean concentration at the height of the velocity maximum ($\overline{c}(H_m)$), and $\overline{c}(z)$ is the mean concentration at distance z above the bed.

Eq. (21) is applicable in the range $0.05H_t < z \leq H_m$ as, due to near-bed deposition, the concentration increases and falls outside the range of the linear relationships of intensity and concentration. So the signal amplitude cannot be used for sediment analysis. Also an ADV has a limitation for measuring signal amplitude in places that are very close to the bed. To the authors' knowledge, Eq. (21) is a new expression for concentration distribution in a turbidity current in a wall region. As it is difficult to obtain reliable concentration data in the wall region (close to the bed) with sampling techniques, no relationship can be found for the concentration distribution in this region in the literature [10].

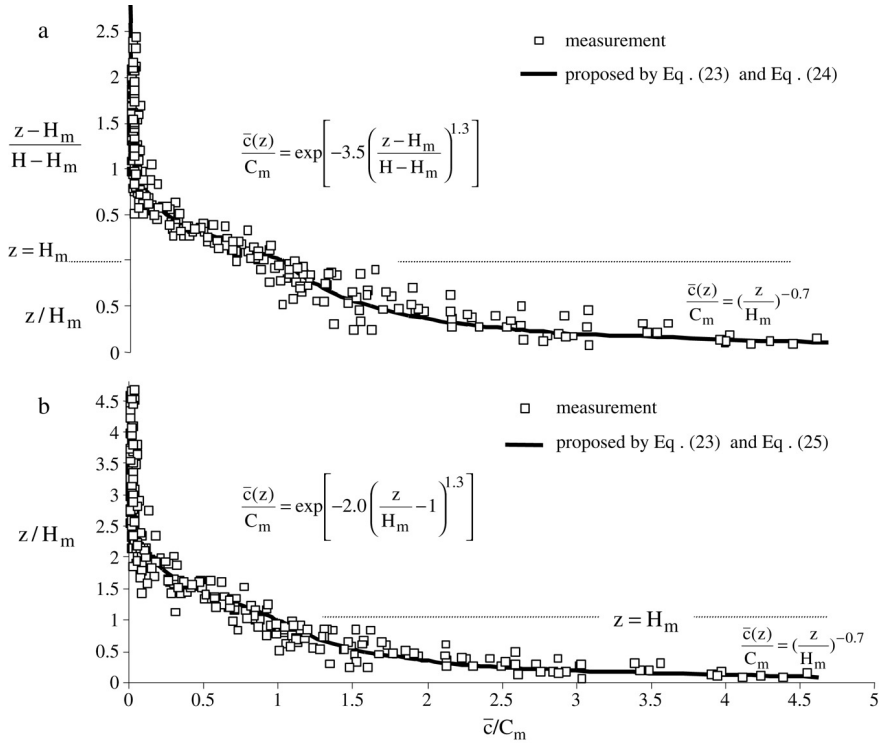

Fig. 6. Dimensionless concentration profile.

A Gaussian-type relation similar to the velocity profiles can approximate the concentration distribution in the outer region:

$$\frac{\overline{c}(z)}{C_m} = \exp\left[-\beta_c\left(\frac{z-H_m}{H-H_m}\right)^{\gamma_c}\right] \tag{22}$$

where β_c is a coefficient, γ_c is an empirical exponent and H is the depth-average thickness of current.

Eqs. (21) and (22) were fitted to the concentration profiles measured inside the inner and outer regions for different experiments. Best-fit curves with respect to the empirical exponents (α_c and γ_c) and coefficient (β_c) were obtained using the least squares method. The result curves show that α_c, γ_c, and β_c have values in the ranges of 0.4 to 0.95, 1.03 to 1.65, and 2.25 to 4.5, respectively. If average values of these coefficients are used, the inner and outer concentration profiles can be simplified as follows:

$$\frac{\overline{c}(z)}{C_m} = \left(\frac{z}{H_m}\right)^{-0.7} \tag{23}$$

$$\frac{\overline{c}(z)}{C_m} = \exp\left[-3.5\left(\frac{z-H_m}{H-H_m}\right)^{1.3}\right]. \tag{24}$$

Replacement of the average current thickness with the height of maximum velocity ($H = 2.6H_m$) results in a simplified form of Eq. (24):

$$\frac{\overline{c}(z)}{C_m} = \exp\left[-2.0\left(\frac{z}{H_m}-1\right)^{1.3}\right]. \tag{25}$$

Summation of Eq. (23) and (25) (or (21) and (22)) leads to a profile for the entire flow:

$$\begin{cases} \omega(\eta) = (\eta)^{-0.7}\psi(1-\eta) \\ \qquad + \exp\left[-2.0\,(\eta-1)^{1.3}\right]\psi(\eta-1) \\ \psi(1-\eta) = \begin{Bmatrix} 1 & \eta < 1 \\ 0 & \eta > 1 \end{Bmatrix} \end{cases} \tag{26}$$

where $\eta = \frac{z}{H_m}$, $\omega = \frac{\overline{c}}{C_m}$ and ψ is the unit step function or Heaviside function.

Eq. (26) is similar to the equation for the velocity profile (Eq. (8)). Estimated dimensionless concentration distributions have been compared with the proposed concentration profile through Eq. (26) in Fig. 6b. Good agreement between Eq. (26) and the measured concentration can be observed.

Direct measurement of the total height of the turbidity current (H_t) is very difficult because there is no clear interface between the dense current and ambient fluid. The estimated concentration at the shear layer between the turbid water and ambient fluid and inside the sediment-diffused ambient fluid (backflow) is nearly zero, whereas concentration values drop rapidly outside of the dense layer current, so the resulting concentration profiles can be successfully used to determine the actual dense layer height. The actual dense layer heights based upon concentration profiles are introduced where the concentration is approximately zero and this height is usually less than the vertical extent of the motion. The proposed concentration profile of Eq. (26) is valid for the

entire flow (inner, outer, and shear–diffusion regions) and this equation asymptotes to zero in the shear–diffusion layer and upper region. The dimensionless concentration profile shows that measurement data for inside the inner region exhibit a little scatter, because of the disturbance of the current during the ADV probe movements.

Successful estimation of the concentration by acoustic backscattering analysis shows promise for this technique as an appropriate tool for determining sediment fluctuations and temporal variations of concentration in deposition and erosion processes.

5. Conclusion

A series of laboratory experiments were conducted to investigate the flow structure in low density turbidity currents. In these experiments the ADV was used to get synchronous information about the mean and instantaneous velocity and the sediment concentration.

It is shown that the ADV provides an excellent opportunity to study the dynamics of sediment-laden gravity currents. It has a number of advantages over other instruments: providing three-axis velocity measurements without interfering with the current, enabling precise distance measurements between the sampling volume and boundary, good penetration in turbid water, and, most importantly, being consistent in velocity and concentration measurements, i.e., they are measured with the same sampling volume. This methodology holds promise and will help to investigate the links between entrainment, transport, and deposition through density fluctuations in these currents.

Velocity and concentration profiles from these experiments are in good agreement with other experimental research [4,10]. Also it is observed that the measured velocity and concentration can be reasonably well represented by similarity profiles.

On the basis of the backscattering intensity from ADV data, the concentration can be estimated in the inner region of the current close to the bed where collecting samples to determine the concentration is very difficult and previous studies could only obtain two or three samples. So a reliable expression for the concentration distribution was proposed for the inner region of particle-laden gravity currents.

References

[1] A.E. Hay, Turbidity currents and submarine channel formation in Rupert inlet, J. Geophys. Res. 92 (1987) 2883–2900.
[2] M.H. Garcia, Depositional turbidity currents laden with poorly sorted sediment, J. Hydr. Eng. 120 (1994) 1240–1263.
[3] G.V. Middleton, Experiments on density and turbidity currents, Can. J. Earth Sci. 3 (1966) 523–546.
[4] B.C. Kneller, C. Buckee, The structure and fluid mechanics of turbidity currents, Sedimentology 47 (2000) 62–94.
[5] C. Buckee, B. Kneller, J. Peakall, Turbulence structure in steady, solute-driven gravity currents. Sediment transport and deposition by particulate gravity currents, Spec. Publ. Int. Assoc. Sediment (2001) 173–189.
[6] B.C. Kneller, S.J. Bennett, W.D. McCaffrey, Velocity and turbulence structure of gravity currents and internal solitary waves, Sediment. Geol. 122 (1997) 235–250.
[7] B.C. Kneller, S.J. Bennett, W.D. McCaffrey, Velocity structure, turbulence and fluid stresses in experimental gravity currents, J. Geophys. Res. 104 (1999) 5281–5291.
[8] R.E. Britter, P.F. Linden, The motion of the front of a gravity current traveling down an incline, J. Fluid Mech. 91 (1980) 531–543.
[9] T.H. Ellison, J.S. Turner, Turbulent entrainment in stratified flows, J. Fluid Mech. 6 (1959) 423–448.
[10] M.S. Altinakar, W.H. Graf, E.J. Hopfinger, Flow structure in turbidity currents, J. Hydr. Res. 34 (1996) 713–718.
[11] M.H. Garcia, G. Parker, Experiments on the entrainment of sediment into suspension by dense bottom current, J. Geophys. Res. 98 (1993) 4793–4807.
[12] M. Garcia, G. Parker, Experiment of bed sediment into suspension, J. Hyd. Eng. 117 (1991) 414–435.
[13] R.E. Britter, J.E. Simpson, Experiments on the dynamics of a gravity current head, J. Fluid Mech. 88 (1978) 223–240.
[14] J.D. Parsons, Mixing mechanisms in density intrusions. Ph.D. Thesis, University of Illinois at Urbana-Champaign, 1998.
[15] R.W. Sterberg, G.C. Kineke, R. Johnson, An instrument system for profiling suspended sediment, fluid, and flow conditions in shallow marine environments, Cont. Shelf Res. 11 (1991) 109–122.
[16] R.L Soulsby, Selecting record length and digitization rate for near bed turbulence measurements, J. Phys. Oceanography 10 (1980) 208–219.
[17] J. Best, A.D. Kirkbride, J. Peakall, Mean flow and turbulence structure of gravity currents. Sediment transport and deposition by particulate gravity currents, Spec. Publ. Int. Assoc. Sediment (2001) 159–173.
[18] A.E. Hay, On the remote acoustic detection of suspended sediment at long wavelengths, J. Geophys. Res. 88 (1983) 7525–7542.
[19] C. Libicki, K.W. Bedford, J.F. Lynch, The interpretation and evaluation of a 3-MHz acoustic backscatter device for measuring benthic boundary layer sediment dynamics, J. Acoust. Soc. Am. 85 (1989) 1501–1511.
[20] F.R. Hess, K.W. Bedford, Acoustic Backscatter System (ABSS): The instrument and some preliminary results, Mar. Geol. 66 (1985) 257–280.
[21] D.C. Fugate, C.T. Fredrichs, Determining concentration and fall velocity of estuarine particle populations using ADV, OBS and LISST, Cont. Shelf Res. 22 (2002) 1867–1886.
[22] K. Kawanisi, S. Yokosi, Measurements of suspended sediment and turbulence in tidal boundary layer, Cont. Shelf Res. 17 (1997) 859–875.
[23] K. Kawanisi, Structure of turbulent flow in shallow tidal estuary, J. Hydr. Eng. 130 (2004) 360–370.
[24] V.I Nikora, D.G. Goring, A. Ross, The structure and dynamics of the thin near-bed layer in a complex marine environment, Estuarine, Coastal Shelf Sci. 54 (2002) 915–926.
[25] V.I. Nikora, D.G. Goring, Fluctuation of suspended sediment concentration and turbulent sediment fluxes an open channel flow, J. Hydr. Eng. 128 (2002) 214–224.
[26] E.W. Dietrich, Settling velocity of natural particles, Water Resour. Res. 18 (1982) 1626–1682.
[27] A. Lohrmann, R. Cabrera, N.C. Karus, Acoustic Doppler velocimeter (ADV) for laboratory use, in: Proc., Symposium On Fundamental and Advancements in Hydraulic Measurements, A.S.C.E., New York, 1994, pp. 351–365.
[28] Nortek As, ADV Specification User and Operation Manual, 1999.
[29] A. Lohrmann, Monitoring sediment concentration with acoustic backscattering instruments, Nortek Technical Note No. 3. 2001, pp. 1–5.
[30] M.M. Thevenot, N.C. Kraus, Comparison of acoustical and optical measurements of suspended material in Chesapeake estuary, J. Mar. Env. Eng. 1 (1993) 65–79.